Int. J. Heat Mass Transfer. Vol. 16, pp. 1919–1929. Pergamon Press 1973. Printed in Great Britain

EVAPORATION FROM A POROUS FLOW CONTROL ELEMENT ON A POROUS HEAT SOURCE

R. J. RAIFF and P. C. WAYNER, Jr.

Division of Fluid, Chemical, and Thermal Processes, Rensselaer Polytechnic Institute, Troy, New York 12181, U.S.A.

(*Received* 22 *January* 1973 *and in revised form* 28 *February* 1973)

Abstract—Evaporation from a microporous flow control element on a porous heat source was studied experimentally and theoretically. Interfacial phenomena were used to couple, in a controllable manner, the mass flux and the heat flux in the flow control element. The vapor exhausted through the heat source and was superheated under some of the experimental conditions. A smooth transition between regimes analogous to normal nucleate and film boiling was obtained with some of the designs. The novel heat transfer surface design could be incorporated into a heat exchange system with uses similar to those of a heat pipe.

NOMENCLATURE

$a, b,$ defined in equation (10);
$D,$ diameter [μ];
$h,$ height [m]; heat transfer coefficient [J/m^{2}sK]; latent heat of vaporization [J/kg];
$i,$ $\sqrt{(-1)}$;
$K,$ thermal conductivity [J/msK];
$k,$ permeability [m^2];
$l,$ exhaust channel width [m];
$m, n,$ defined in equation (12);
$M,$ molecular weight [kg/kg-mole];
$p,$ pressure [N/m^2);
$Q_{gen},$ internal heat generation rate [J/sm^3];
$q,$ heat flux [J/sm^2];
$R,$ universal gas constant [Nm/kg-mole°K];
$r,$ blockage ratio—see Fig. 4;
$T,$ absolute temperature [°K]; complex potential function;
$t,$ temperature [°C];
$w,$ mass flux [kg/sm^2];
$X, Y,$ dimensionless coordinates;
$x, y,$ coordinates [m];
$Z,$ complex geometric variable;
$\nabla,$ $\boldsymbol{i}\cdot\frac{\partial}{\partial x}+\boldsymbol{j}\cdot\frac{\partial}{\partial y}$
$\hat{\nabla},$ $rl\nabla$;
$\mu,$ viscosity [Ns/m^2];
$\pi,$ 3·14159;
$\rho,$ density [kg/m^3];
$\sigma_1,$ interfacial resistance coefficient;
$\Phi,$ potential function.

Subscripts

$E,$ externally applied pressure difference;
evap, evaporation;
$hs,$ heat source;
$i,$ incompressible;
$l,$ liquid;
$lv,$ liquid–vapor;
$N,$ dimensionless
o, average integral value based on superficial area of the MPFCE;
$p,$ pore;
$s,$ saturation;
$w,$ mass transfer solution;
$Z,$ complex.

INTRODUCTION

IN AN effort to eliminate some of the undesirable characteristics of boiling a new change-of-phase heat transfer (HTS) has been proposed [1]. This surface which consisted of a porous heat source was later modified by the addition of a porous flow control element [2]. In this combined

arrangement liquid is fed into the flow control element through the surface opposite the heat source and the evaporant is exhausted through the heat source. The feasibility of using such a HTS and some of its operating characteristics have been experimentally studied [2–5]. However, the pore sizes in the flow control elements used in these studies were too large to completely assess the effects of capillary forces on the heat transfer process. One of the objectives of the work presented in this paper was to investigate both experimentally and theoretically, the effects of capillary forces by using a microporous flow control element (MPFCE). Another objective of this study was to design and evaluate a representative HTS that could be easily used in a heat exchanger. The potential uses of this HTS are similar to those of the heat pipe.

QUALITATIVE DISCUSSION OF THE HEAT TRANSFER SURFACE

The HTS surface under study is one for which the flow of an evaporating fluid and its vapor is controlled by a MPFCE. Flow control is accomplished by utilizing the surface forces present at the liquid–vapor interface (LVI) in the multitude of micropore openings at or near the down stream surface of the MPFCE. A cross-sectioned drawing of a portion of the particular configuration used for these studies is presented in Fig. 1. The liquid that is to be evaporated is fed from the liquid reservoir through the MPFCE to the LVI. Simultaneously the energy necessary for evaporation is conducted from the heat source through the MPFCE to the LVI. The resulting vapor is then directed away from the interface in the same direction of flow as the liquid.

The capillary forces associated with the menisci in the micropores serve a threefold function. They direct the flow of the generated vapor, separate the evaporating liquid from its vapor, and control the fluid flow rate. The first two of these effects are achieved by the physical presence of the meniscus and its associated pressure drop. As long as the pressure drop needed to drive the vapor away from the meniscus is less than the maximum pressure drop that the meniscus can support, the vapor flow will be in the desired direction. The third effect is achieved by the ability of the meniscus to change shape, and, therefore, alter the pressure drop across it. As outlined by Potash and

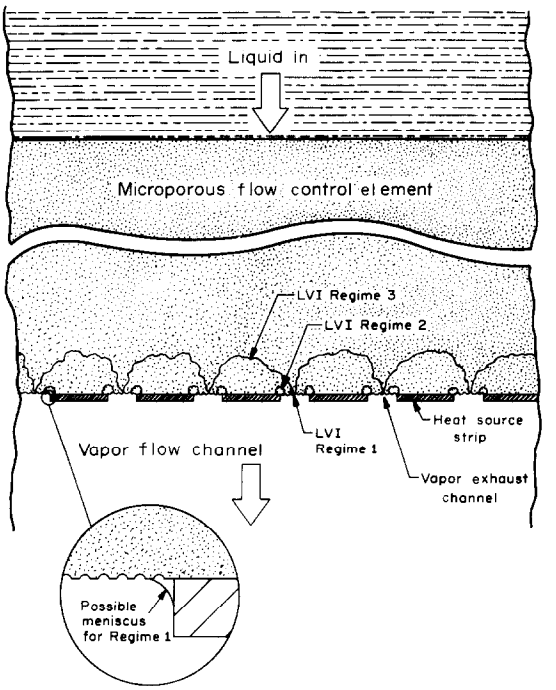

FIG. 1. Cross sectional sketch of heat transfer element.

Wayner [6] increases in the heat flux to the LVI are accommodated by a decrease in the radius of curvature of the menisci. This leads to a lowering of the pressure on the liquid side of the interface with a resulting increase in fluid flow rate. This stable evaporating meniscus is of considerable importance because its presence and location determines the operating characteristics of the heat transfer process. Since the pressure difference across a meniscus, and therefore the entire LVI, is directly proportional to the surface tension and inversely proportional to the radius of curvature, substantial pressure differences are attainable with small pores.

However, the use of small pores to obtain flow control exacts a penalty in the form of a high fluid flow resistance through the MPFCE. Therefore, externally imposed pressures are necessary for high volumetric flow rates in thick porous elements with small pores.

This heat transfer process can be divided into three operating regimes which are analogous to the operating regimes in normal boiling. These are: regime (1), the MPFCE is completely filled with liquid (analogous to nucleate boiling); regime (2) transition; and regime (3) the MPFCE is partially dry, that is a substantial portion of the LVI has moved away from the down stream boundary of the MPFCE (analogous to film boiling). The positions of the LVI for these regimes are presented in Fig. 1. The operating characteristics of these three regimes are different and require independent analyses.

The HTS can be used in a heat exchange process in the following way. The thickness of the "heat source" can be increased with the downstream side placed in contact with a solid surface. This forms vapor exhaust channels running perpendicular to the page. The "heat source" could then be either in contact with a heated solid surface or have an internal heat source. The vapor leaving the channels would be superheated by the walls of the exhaust channels. With the proper design this heat transfer surface would be useful in heat pipe applications.

EXPERIMENTAL STUDIES

The following material was abstracted from a thesis [7] in which a more detailed description of this experimental and theoretical work can be found.

Description of test apparatus

A schematic cross sectional drawing of the test apparatus is presented in Fig. 2. This apparatus consisted of three main sections: (1) the heat transfer element (HTE), (2) a liquid reservoir, and (3) a vapor guide and condenser to contain and collect the generated vapors. The HTE consisted of the MPFCE (porous ceramic disks manufactured by the Coors Porcelain Co.) and the attached heat source (closely spaced parallel strips of copper resistance heaters). This was attached to a sheet of copper clad printed circuit board which served a three-fold function: (1) as bus-bar to supply power to the HTE, (2) as structural support for the HTE, and (3) as the separator between the liquid and vapor sections.

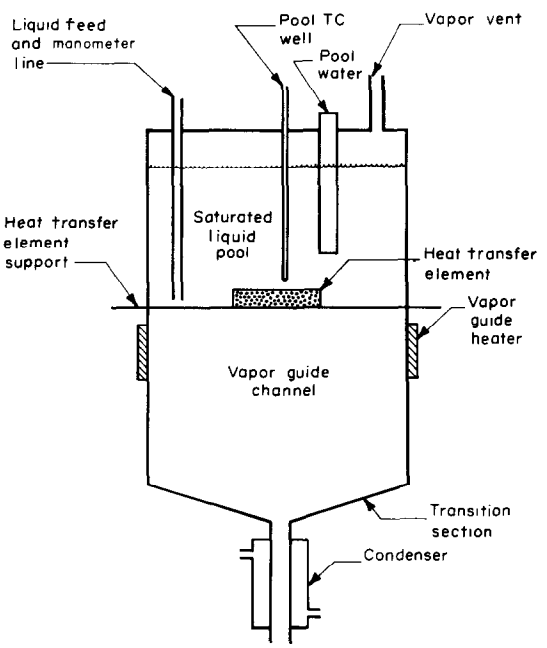

FIG. 2. Schematic cross section of experimental apparatus.

A rectangular channel, equal in size to the active heat transfer area, was cut in the support to allow passage of the evaporated fluid. Two 0·3 m sections of 0·15 m dia Pyrex pipe were used for the liquid reservoir and the vapor guide. The upper end of the liquid reservoir was sealed by a stainless steel plate in which openings were provided for a heater to control the pool temperature, a liquid feed line, a vapor removal line, and a thermocouple to monitor the pool temperature. A funnel was sealed to the lower end of the vapor guide to provide a transition into the condenser. Auxilliary heaters were attached to the vapor guide to control heat

losses from the edges of the HTE and to prevent condensation from obscuring a clear view of the HTE.

The MPFCE were 6 mm thick and 75 mm in diameter. Tests were performed using disks with mean pore diameters of 0·25, 2 and 10 μ. Direct contact between the MPFCE and the heat source was obtained, without the use of adhesives, as follows. First, a conductive layer of copper, in the desired heater pattern, was vapor deposited onto the surface of the disk. Then, the heater pattern was built up to the desired thickness by electroplating. The pattern selected for study consisted of narrow, closely spaced heater strips connected to a common current source at their ends. Two different heater strip widths and spacings were used. One with strips 0·508 mm wide, and spacings 0·254 mm wide, and one with strips 0·254 mm wide and spacings 0·127 mm wide. In all cases the projected heat transfer area was rectangular and approximately 25 mm wide and 50 mm long. The actual dimensions of heat source and flow control element used are presented in Table 1. The temperature distribution on the surface of the HTE was measured using fine wire copper–constantan thermocouples. The average temperature of the HTE was determined by using the heating element as a resistance thermometer. The d.c. power to the resistance heater was supplied from an 18 kW Rapid Electric d.c. power supply. Voltage regulation was maintained to ±2 per cent of nominal setting and ripple was less than 1 per cent of the d.c. output. The voltage drop across the HTE, the current through the HTE (using a constant resistance series shunt), and the millivolt output of the thermocouples were all measured using a Honeywell Electronic 19 two-channel potentiometric Lab. recorder. The volume of condensate and its collection time were also measured. For comparison the flow through the MPFCE, due to the externally applied pressure, was measured before energizing the power supply.

Method of operation

The liquid reservoir was filled with either

Table 1. Experimental configurations

Data set	Fluid	Mean pore size (μ)	Heat source strip width (m × 10^4)	Number of heat source strips	Vapor exhaust channel width (m × 10^4)	Externally applied pressure (N/m²)	Permeability (m² × 10^{16})	Apparent porosity (% of volume)
4–1	methanol	2	5·08	32	2·59	2442	52·2	42·1
5–1	↓	10	↓	↓	↓	2442	478	45·7
5–2	↓	↓	↓	↓	↓	1484	478	↓
5–3	↓	↓	↓	↓	↓	2442	219	↓
5–4	↓	↓	↓	↓	↓	4884	219	↓
5–5	↓	↓	↓	↓	↓	9767	219	↓
6–1	↓	0·25	2·59	64	1·29	2059	1·57	34·3
7–1	water	2	5·08	32	2·59	3830	52·2	42·1
7–2	↓	↓	↓	↓	↓	6224	52·2	↓
7–3	↓	↓	↓	↓	↓	8618	52·2	↓

Microporous flow control element thickness = 6 mm.
Superficial heat transfer dimensions 25 mm × 50 mm.
Thermal conductivities of the MPFCE (J/msK)

D_p	Dry	Liquid filled
10	1·07	1·90
2	1·02	1·73
0·25	0·62	1·35

filtered deionized water or methanol to a predetermined depth that was maintained constant during a test run. The vapor exhaust guide and condenser were vented to atmosphere. The pool and vapor guide heaters were then adjusted to heat the liquid pool and heat transfer zone to the desired saturation temperature. When this temperature stabilized the main power supply was turned on to energize the HTE. Once the power level had been set, the thermocouples on the HTE were monitored on the recorder until the HTE temperature stabilized. As soon as steady state was reached (no temperature change over a period of 15 min) the condensate was collected for periods greater than 30 min and measured. Concurrent records of the HTE voltage drop and the standard shunt voltage drop were made so that the power and average temperature were easily calculated.

Data reduction and error analysis

Since the temperature differences in the heat transfer process studied were initially the same order of magnitude as the standard errors associated with thermocouple and resistance temperature measurements, all temperature sensors were individually calibrated using a constant temperature bath and a NBS calibrated platinum resistance thermometer. The maximum error in reading the thermocouple temperatures was $\pm 0{\cdot}25$ per cent of the centigrade temperature and the maximum error in reading the average HTE temperature, using the heater as a resistance thermometer, was $\pm 0{\cdot}37$ per cent of the centigrade temperature. The error in the measured weight flow was negligible. The determination of the energy input to the HTE was accurate to $\pm 0{\cdot}36$ per cent. The measurement of the superficial area of the active portion of the HTE was accurate to $\pm 0{\cdot}1$ per cent.

An examination of the data for HTE's 4, 5 and 7 showed that in the 100 per cent vapor quality region of operation, the heat flux calculated from the energy input differed from the heat flux calculated from the weight flow by less than 5 per cent. It was assumed that the heat balance would be at least as good in the region where the vapor quality was less than 100 per cent, because of the smaller temperature gradients in this region. Therefore, for vapor qualities less than 100 per cent the evaporative heat flux was taken as equal to the energy input. For HTE 6, even though operation was always in the 100 per cent vapor quality region, the energy absorbed at the LVI only accounted for 45 per cent of the heat generated. However, a theoretical analysis [7] showed that, in this case, the LVI temperature was so much above the pool saturation temperature that the heat loss to the liquid pool amounted to approximately 50 per cent of the heat generated and only about 5 per cent of the energy flow was not accounted for.

Experimental results

The reduced data are presented in Fig. 3. In this figure the average heat flux based on superficial area, q_0, is presented as a function of the average temperature difference between the

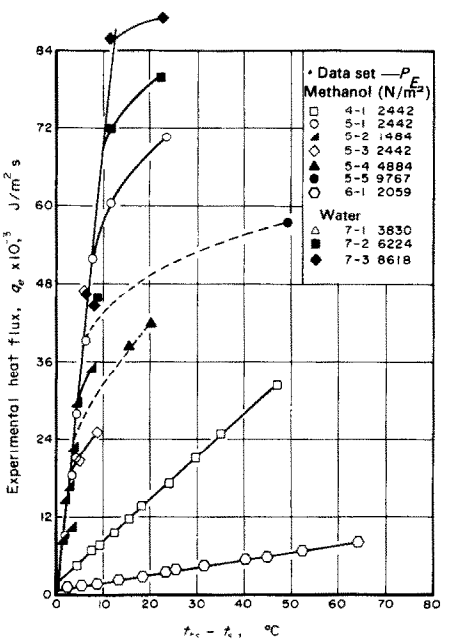

FIG. 3. Experimental heat fluxes.

heat source and the one atmosphere saturation temperature, $(t_{hs} - t_s)$. The almost vertical straight line goes through the data taken in heat transfer regime 1. In this regime the vapor quality varied between 0 per cent at low $t_{hs} - t_s$ and 100 per cent near the beginning of transition. The various points at which the individual curves branch off represent the beginning of regime 2. The vapor quality always reached 100 per cent before this point. Examination of the experimental data demonstrates that the heat flux level at which transition begins is a function of the fluid supply rate and the heat of vaporization. The fluid supply rate is a function of several variables which includes the permeability of the microporous element, the externally applied pressure difference, the viscosity and density of the fluid, and the capillary suction potential. The effect of varying only the fluid can be seen by comparing data sets 4-1 and 7-2. The analysis presented in [7] confirms that this large difference in behavior is to be expected. Comparison of data sets 5-1 with 5-2, and 5-3 with 5-4 and 5-5, shows the effect of changing only the externally applied pressure. Comparison of 5-1 with 5-3 shows the effect of a change in permeability with all other variables held constant. Data sets 4-1 and 6-1 show the behavior of the heat transfer system as the LVI moves into the MPFCE. The difference in the slopes of these two data sets can be accounted for by two factors: (1) the thermal conductivity of the MPFCE used in set 4-1 was twice that of the element used in data set 6-1; and (2) the LVI temperature for data set 6-1 was much higher than that for data set 4-1. The second factor was due to the large difference in the pressures needed to exhaust the vapor through the two different elements. Therefore, the saturation temperature at the LVI was well above the one atmospheric saturation temperatures and significant energy was conducted to the upper surface of the MPFCE. Data set 4-1 shows that a moderate range of capillary suction control can be attained while maintaining a heat flux level comparable to that of data sets 5-1 through 5-5 which were run with a higher permeability flow control element. The last stable point in data set 4-1 represents a weight flow 6·5 times the weight flow possible with the externally applied pressure (assuming no capillary suction). Due to the lower permeability, the maximum heat flux attained in data set 6-1 was much lower than that attained in other runs. However, this data set demonstrates the wide range of stable operation possible when very small pores are used. The last stable point in data 6-1 represents a weight flow approximately 60 times the weight flow due to the externally applied pressure (assuming no capillary suction).

Visual observations made during the course of the experiments showed the following: (1) At the heat flux level where the mass flux first started to increase (approx. 10 per cent vapor quality), the surface of the vapor exhaust channel was still covered by a thin film of liquid; (2) there was no vapor evolution from the upper surface for HTE 4, 6 and 7; (3) at the higher heat flux levels, there was some vapor evolution from the upper surface of HTE 5. The first of these observations indicate that capillary suction and the inception of transition begins in a very narrow region adjacent to the heat source–vapor exhaust channel interline. Examination of the mass flow data showed the following: (1) as expected the mass flux for HTE 4 and 6 increased with increasing heat flux; (2) this was also true of HTE 5 in the high vapor quality region; and (3) in the low vapor quality region of operation, HTE 5 exhibited a decrease in mass flux with increasing heat flux. This initial decrease in mass flux and the later observed evolution of vapor from the upper surface of HTE 5 leads to the hypothesis that this behavior was due to the formation of vapor pockets in the flow control element. This would be more evident for HTE 5 than for other elements because HTE 5 had the largest pores combined with the fluid with a lower surface tension. Examination of the data for HTE 7 showed that there was much less of an increase in mass flux due to capillary suction than expected. Subse-

quent testing demonstrated that the MPFCE was poorly wetted by water.

Of all the previous data taken for this type of heat transfer surface the experimental design used in these studies was most similar to design "A" of reference [5]. However, the following major differences prevent direct numerical comparison: (1) the pore size in the MPFCE was much larger in [5]; (2) in [5] the contact between the MPFCE and the heat source was provided by physical pressure whereas in these studies the heat source was deposited directly onto the MPFCE; and (3) in [5] vapor exhaust channels below the MPFCE was provided by a pattern of circular holes in the heat source, whereas in these studies the vapor exhaust channels were parallel rectangular spaces between the heater strips. Nevertheless, the mode of operation and heat transfer characteristics of the HTE were similar.

ANALYTICAL STUDIES

The symmetry of the experimental configuration is utilized to reduce the area for analysis to the two dimensional region presented in Fig. 4.

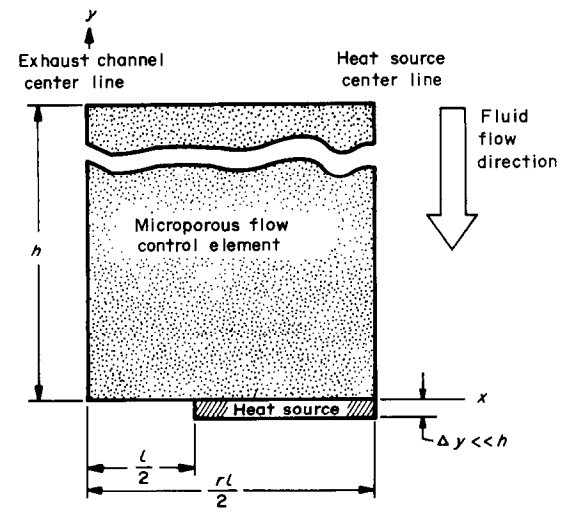

FIG. 4. Cross sectional drawing of analytic model.

In order to reduce the analysis to manageable proportions the MPFCE surface between the heating strips and the LVI are assumed to be at constant potential whenever possible. For the fluid flow analysis this assumption is exact at the MPFCE surface between the heating strips when there is uniform pressure (liquid flow, either with no capillary suction or with uniform capillary suction, and when there is vapor flow). In all other cases it is only true in an average sense. This assumption cannot be used for the heat flux analysis as long as the LVI is in contact with the heat source-exhaust channel interline, for it would require a step change in the temperature at the interline. A finite difference solution is used for this case. The following solution is for Regime 1 during which the MPFCE is completely filled with liquid.

Equation (1) is the differential equation for the pressure distribution in the porous media based on the following assumptions: (1) two dimensional incompressible steady flow; (2) no sources or sinks; (3) the Darcy relationships between superficial velocity and pressure drop for flow in porous media apply; and (4) the fluid viscosity is independent of temperature [8].

$$\frac{\partial}{\partial x}\left[\frac{k}{\mu}\frac{\partial p}{\partial x}\right]+\frac{\partial}{\partial y}\left[\frac{k}{\mu}\left(\frac{\partial p}{\partial y}+\rho g\right)\right]=0. \quad (1)$$

If we now define the dimensionless quantities $X = x/rl$, $Y = y/rl$, $\hat{\nabla} = rl\nabla$, and the dimensionless mass flow potential,

$$\Phi_{Nwi}=\frac{\rho k}{rlw_0\mu}(p+\rho grly) \quad (2)$$

equation (1) becomes

$$\hat{\nabla}^2\Phi_{Nwi}=0. \quad (3)$$

The boundary conditions for equation (3) are

$$X=0 \text{ or } \tfrac{1}{2},\ 0\leqslant Y\leqslant h/rl;\quad \partial\Phi_{Nwi}/\partial X=0 \quad (4)$$

$$0\leqslant X\leqslant \tfrac{1}{2},\ Y=h/rl;\quad \partial\Phi_{Nwi}/\partial Y=1 \quad (5)$$

$$0\leqslant X<\tfrac{1}{2}r,\ Y=0;\quad \Phi_{Nwi}=\text{constant} \quad (6)$$

$$\tfrac{1}{2}r<X\leqslant\tfrac{1}{2},\ Y=0;\quad \partial\Phi_{Nwi}/\partial Y=0. \quad (7)$$

The solution to this mass flow problem can be effected using the methods of conformal transformation due to Schwarz and Christoffel [9, 10]. Using $Z = X + iY$, the complex physical variable, and $T_{Nw} \equiv \Phi_{Nw} + i\Psi_{Nw}$, the complex potential variable, the solution is

$$T_{Nw} = \frac{1}{\pi}\cosh^{-1}\left[\frac{\sin(\pi Z)}{\sin(\pi/2r)}\right]. \quad (8)$$

The desired solution is the real part of equation (8)

$$\Phi_{Nw} = \frac{1}{\pi}\cosh^{-1}\left[\frac{a+b}{2}\right] \quad (9)$$

where

$$a = [(1+m)^2 + n^2]^{\frac{1}{2}} \text{ where } a \text{ and } b \text{ must be the positive root} \quad (10)$$

$$b = [(1-m)^2 + n^2]^{\frac{1}{2}} \quad (11)$$

and

$$m = \sin \pi X \cosh \pi Y / \sin(\pi/2r) \quad (12)$$

$$n = \cos \pi X \sinh \pi Y / \sin(\pi/2r).$$

The complex mass flux ratio, $(w/w_0)_Z$ may be obtained from [11]

$$\left(\frac{w}{w_0}\right)_Z = \frac{dT_{Nw}}{dz}. \quad (13)$$

Using equation (13) and evaluating the result at $Y = 0$ gives us the mass flux distribution ratio at the surface of the MPFCE between the heater strips,

$$\left(\frac{w}{w_0}\right)_{Y=0} = \frac{\cos(\pi X)}{[\sin^2(\pi X) - \sin^2(\pi/2r)]^{\frac{1}{2}}} \quad (14)$$

where w_0 is the undisturbed mass flux at $Y = h/rl$ and is a function of the sum of the external pressure drop and capillary suction. A plot of this distribution is presented in Fig. 5. The blockage ratio, r, of 3 is the theoretical blockage ratio for the experiments that were performed. The mass flux ratios listed in Fig. 5 are those at a point one pore radius away from the heater–exhaust channel interline for each of the three average pore diameters used. Unfortunately since the Darcy assumptions no longer apply when the averaging volume is the same order of magnitude as the pore diameter, the mass flux ratio loses meaning as the heat source is approached. Nevertheless, the results are useful in this region in that they demonstrate the converging nature of the flow field.

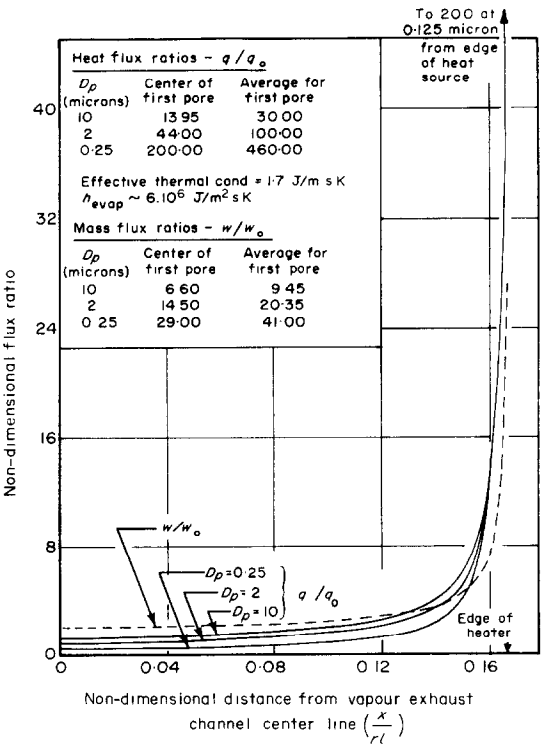

FIG. 5. Flux distribution across the exhaust channel surface for a blockage ratio of 3.

Equation (15) is the two dimensional steady state differential equation for heat flow in both the porous media and the heat source assuming that the local fluid and solid temperatures are equal.

$$K\nabla^2 t + Q_{gen} = 0 \quad (15)$$

the boundary conditions are

$$x = 0, 0 \leqslant y \leqslant h; \partial t/\partial x = 0 \quad (16)$$

$$x = rl/2, -\nabla y \leqslant y \leqslant h; \partial t/\partial x = 0 \quad (17)$$

$$x = l/2, -\Delta y \leqslant y \leqslant 0; \partial t/\partial x = 0 \quad (18)$$

$$0 \leqslant x \leqslant rl/2, y = h; \partial t/\partial y = 0 \quad (19)$$

$$0 \leqslant x < l/2, y = 0; K(\partial t/\partial y) = h_{evap}(t_{tv} - t_s) \quad (20)$$

$$l/2 \leqslant x \leqslant rl/2, y = -\Delta y; \partial t/\partial y = 0. \quad (21)$$

For evaporation at a LVI the heat transfer coefficient can be represented by [12]

$$h_{evap} = \sigma_1 \left[\frac{M}{2\pi R\bar{T}}\right]^{\frac{1}{2}} \frac{h_{tv}^2 \rho_v}{T_s}. \quad (22)$$

Except for equation (18), the boundary conditions are straightforward. There are two possible limits for the boundary condition on this surface. One is to consider the surface with a meniscus on it and the other is to consider it dry. The first of these two possible boundary conditions when used in the analysis demonstrated that contrary to the experimental results the average HTE temperature did not rise appreciably above the saturation temperature. Upon analytically examining the possibilities for the dry surface approximation, it was found that unless the heat transfer coefficient was large (on the order of 10^4 J/m^{2}sK) the calculated average temperature of the HTE was not affected appreciably by changes in the coefficient. Therefore, to simplify the analysis the surface was taken as adiabatic. These results demonstrate the importance of the location of the evaporating meniscus.

Equation (15) was solved using a numerical "relaxation" technique on a digital computer. In the MPFCE a minimum grid dimension at the corner was chosen to be one mean pore diameter, because it is a characteristic dimension of the porous media. Physically this assumer that the first node at the surface of the porous media in the vapor exhaust channel next to the heat source represents an average pore with a uniform flux and temperature. Further, the fluid distribution in the pore can self-adjust as a result of surface forces to match the real variation in the heat flux across the pore. As a result of this choice the heat flux profile on the exhaust channel surface was a function of pore size. The size of the nodes surrounding the corner node were varied to assure a converged solution. The dimensionless heat flux distributions across the vapor exhaust channel surface, calculated using the numerical relaxation program, are presented in Fig. 5. The average flux based on the superficial area is

$$q_0 = Q_{gen}\left(\frac{r-1}{r}\right)\Delta y. \quad (23)$$

The use of the effective thermal conductivity (the numerical values based on experimental measurements made using liquid filled samples of the MPFCE are given in Table 1), and the differential equation for the temperature distribution to calculate the heat flux ratio in the region right next to the heat source is more meaningful than the calculation of the mass flux ratios. Comparison of the results presented in Fig. 5 demonstrates the way the process was mass flow limited at the corner for a given average mass flow rate. Once this mass flux limit has been reached, further increases in the heat flux will cause the LVI to recede from the bottom surface. Because of the increased conduction distance from the heat source to the LVI, the slope of the average heat flux, q_0, vs the temperature difference, $t_{hs} - t_s$, will decrease and transition to regimes two and three will occur. Preliminary analyses [7] of these regimes, which is beyond the scope of the present paper, indicate that the LVI profiles are as presented in Fig. 1.

COMPARISON OF EXPERIMENTAL AND THEORETICAL RESULTS

The comparison between the theory and the experimental results for regime 1 is based on the constant heat transfer coefficients. These coefficients are as follows: For $D_p = 10\,\mu$, the theoretical coefficient is 6530 J/m^{2}sK and the experimental coefficient is 6439 J/m^{2}sK. For $D_p = 2\mu$, the theoretical coefficient is 8347 J/m^{2}sK, and the experimental coefficient is 6882 J/m^{2}sK. For $D_p = 0{\cdot}25\mu$, the theoretical coefficient is

11357 J/m^{2}sK. Due to the extremely low value of the critical heat flux for the 0·25μ element, it was not possible to obtain experimental data in this operating regime. Comparison of the experimental and theoretical results demonstrates that the liquid was not in contact with the edge of the heat source. Otherwise the average temperature of the HTE would have been much lower. This is reasonable since the menisci adjacent to the interline must recede to the porous element to provide suction for the fluid flow.

CONCLUDING REMARKS

An examination of the heat flux distribution at the exhaust channel surface, leads to the conclusion that approximately 50 per cent of this energy is removed in 20 per cent of the exhaust channel adjacent to the heat source. Therefore, the overall efficiency of the heat transfer process can be increased if the fraction of the total evaporating area close to the heat source is increased. This could be accomplished either by producing narrower, more closely spaced, heater strips in the present configuration, or by altering the configuration. It should be emphasized that the present design did not maximize the performance of the HTE because the MPFCE was chosen for experimental convenience and was very thick and had a low thermal conductivity. An increase in the thermal conductivity of the MPFCE would give a more uniform heat flux distribution across the exhaust channel and, therefore, a higher average heat flux before the inception of transition. Since the process is mass flow limited a decrease in the fluid flow resistance, due to an increase in permeability or the use of a thinner MPFCE, would further enhance the process. The use of a working fluid with a higher surface tension, such as liquid metals, would also enhance the mass flow and increase the heat flux attainable before the inception of transition.

Comparison of the theory and the experimental result leads to the following conclusions:

(1) The heat flux characteristics of this process are a function of the HTE geometry and properties, the fluid properties, and the heat flux level.
(2) The forces associated with capillarity were successfully utilized to couple the mass flux and heat flux at the LVI.
(3) The use of micropores in the MPFCE gave a region of operation in which 100 per cent vapor product quality was obtained without the use of "non-wetting" materials.
(4) The inception of transition in the present configuration with micropores did not exhibit the type of burnout characteristic of this transition in boiling.
(5) The analytical model accurately describes the heat transfer process when the MPFCE is completely filled with liquid.

ACKNOWLEDGEMENT

The support of N.S.F. Grant# GK-24227 entitled "Heat and Mass Transfer in Evaporating Menisci" is gratefully acknowledged.

REFERENCES

1. S. G. Bankoff, Taylor instability of an evaporating plane interface, *A.I.Ch.E. Jl* 7, 485–487 (1961).
2. P. C. Wayner, Jr. and S. G. Bankoff, Film boiling of nitrogen with suction on an electrically heated porous plate, *A.I.Ch.E. Jl* 11, 59–64 (1965).
3. V. K. Pai and S. G. Bankoff, Film boiling of nitrogen on an electrically heated horizontal porous plate: effect of flow control element porosity and thickness, *A.I.Ch.E. Jl* **11**, 65–69 (1965).
4. V. K. Pai and S. G. Bankoff, Film boiling of liquid nitrogen from porous surfaces with vapor suction, *A.I.Ch.E. Jl* **12**, 727–736 (1966).
5. P. C. Wayner, Jr. and A. S. Kestin, Suction nucleate boiling of water, *A.I.Ch.E. Jl* **11**, 858–865 (1965).
6. M. Potash, Jr. and P. C. Wayner, Jr., Evaporation from a two-dimensional extended meniscus, *Int. J. Heat Mass Transfer*, **15**, 1851–1863 (1972).
7. R. J. Raiff, An experimental and theoretical investigation of suction boiling, Doctors Thesis, Rensselaer Polytechnic Institute (June 1972).
8. M. Muskat, *The Flow of Homogeneous Fluids Through Porous Media*. McGraw-Hill, New York (1937).
9. R. V. Churchill, *Introduction to Complex Variables and Applications*. McGraw-Hill, New York (1948).
10. R. E. Collins, *Flow of Fluids Through Porous Materials*. Rheinhold, New York (1961).
11. W. J. Gibbs, *Conformal Transformations*. Chapmann & Hall, London (1958).
12. K. Nabavian and L. A. Bromley, Condensation coefficient of water. *Chem. Engng Sci.* **18**, 651–660 (1963).

EVAPORATION DEPUIS UN ELEMENT POREUX DE CONTROLE D'ECOULEMENT PLACE SUR UNE SOURCE POREUSE DE CHALEUR

Résumé—On a étudié expérimentalement et théoriquement l'évaporation depuis un micro-élément poreux de contrôle d'écoulement sur une source poreuse de chaleur. Des phénomènes d'interface ont été utilisés afin de coupler de manière contrôlable le flux massique et le flux thermique dans l'élément de contrôle. La vapeur évacuée à travers la source de chaleur est surchauffée dans quelques conditions expérimentales. On a obtenu dans certains cas une transition douce entre des régimes semblables à l'ébullition nucléée normale et à l'ébullition en film. La nouvelle réalisation pourrait être incorporée à un système d'échange de chaleur comparable aux caloducs.

VERDAMPFUNG VON EINER PORÖSEN STRÖMUNGSFÜHRUNG AN EINER PORÖSEN WÄRMEQUELLE

Zusammenfassung—Die Verdampfung von einer feinporösen Strömungsführung an einer porösen Wärmequelle wurde experimentell und theoretisch untersucht. Grenzschichtphänomene wurden benutzt, um in einer bestimmten Weise Massenstrom und Wärmestrom in der Strömungsführung zu verbinden. Bei einigen Versuchen war der Dampf, der aus der Wärmequelle ausströmte, überhitzt. Bei einigen Anordnungen erhielt man einen glatten Übergang zwischen Zuständen ähnlich dem Blasensieden und dem Filmsieden. Die neue Ausführung der Wärmeübergangsfläche in einem Wärmeaustauschsystem könnte ähnlich wie ein Wärmerohr verwendet werden.

ИСПАРЕНИЕ ИЗ ПОРИСТОГО ЭЛЕМЕНТА, РЕГУЛИРУЮЩЕГО ТЕЧЕНИЕ НА ПОРИСТОМ ИСТОЧНИКЕ ТЕПЛА

Аннотация—Проведено экспериментальное и теоретическое исслкдование испарения из микропористого элемента, регулирующего течение на пористом источнике тепла. Взаимосвязь массового и теплового потоков в элементе регулирования течения достигалась за счет использования явлений на границе фаз. Пар выпускался через источник тепла и затем перегревался при определенных экспериментальных условиях. С помощью специальных устройств достигнут плавный переход от одного режима к другому, которые аналогичны обычному пузырьковому и пленочному кипению. Поверхность теплообмена новой конструкции можно использовать в теплообменниках с той же целью, что и тепловые трубки.